In vivo drug distribution dynamics in thermoablated and normal rabbit livers from biodegradable polymers

Jinming Gao,[1] Feng Qian,[1] Agata Szymanski-Exner,[1] Nicholas Stowe,[2] John Haaga[3]
[1]*Cancer-Targeted Drug Delivery Laboratory, Department of Biomedical Engineering, Case Western Reserve University, Cleveland, Ohio 44106*
[2]*Department of Surgery, School of Medicine, Case Western Reserve University, Cleveland, Ohio 44106*
[3]*Department of Radiology, University Hospitals of Cleveland, Cleveland, Ohio 44106*

Received 15 October 2001; revised 14 February 2002; accepted 14 February 2002

Abstract: Image-guided radiofrequency ablation combined with intratumoral drug delivery provides a novel and minimally invasive treatment of liver cancers. In this study, the *in vivo* transport properties of doxorubicin in thermoablated and nonablated rabbit livers were characterized and compared. Doxorubicin was released from polymer implants (millirods) to the ablated and nonablated liver tissue. At different time points, the 2D distribution profiles were quantitatively determined by a fluorescence imaging method. Analysis of the doxorubicin concentration at the ablation boundary showed that it reached a maximum of 49.8 μg/g at 24 h after implantation, which was higher than the reported cytotoxic concentration of doxorubicin (6.4 μg/g) for liver VX-2 cancer cells. This value dropped to 0.4 μg/g at 48 h after implantation due to the depletion of doxorubicin from the polymer millirod. Results also showed that the area of drug distribution was significantly larger in ablated tissue than nonablated tissue. The therapeutic penetration distance was found to be 5.2 mm in thermoablated livers, compared to 1.2 mm in nonablated livers at 24 h. This difference in drug transport properties is attributed to destruction of the vasculature network in the ablated tissue as supported by histological analysis. Consequently, drug washout by blood perfusion is hampered while drug diffusion becomes the dominant process of transport in the ablated tissue. Results from this study provide insightful information on the rational design and development of polymer millirods for intratumoral drug delivery applications. © 2002 Wiley Periodicals, Inc. J Biomed Mater Res 62: 308–314, 2002

Key words: intratumoral drug delivery; Poly(D,L-lactide-*co*-glycolide); *in vivo* drug transport; RF ablation; polymer implants

INTRODUCTION

Image-guided radiofrequency (RF) ablation of solid tumors is emerging as a powerful, minimally invasive technique for the treatment of human cancers.[1–3] This procedure relies on the advanced imaging techniques (e.g., computed tomography, magnetic resonance imaging), which permit accurate placement of a needle electrode inside solid tumors to destroy the tumor tissue by heat. RF tumor ablation is currently under phase II clinical trials at Case Western Reserve University and University Hospitals of Cleveland.[1] As part of the clinical trials, it has been used to treat cancers of the liver, pancreas, breast, and prostate. Compared to surgical resection, image-guided RF ablation provides a more patient-compliant and much less costly treatment. Its application, however, is currently limited due to the incomplete elimination of all the cancer cells at the ablation boundary, which leads to tumor recurrence and requires repeated treatments.[4,5]

The long-term goal of our research is to develop a combination therapy, which consists of RF tumor ablation followed by intratumoral drug delivery, to achieve the total control of the liver cancer. In this paradigm, image-guided RF ablation will first provide instantaneous destruction of the majority of the liver tumor by heat. After RF ablation, a drug-loaded polymer millirod (diameter 1.6 mm) will be directly implanted inside the ablated tumor by a modified 14-gauge tissue biopsy needle under image guidance. Intratumoral drug delivery will then provide a sustained local chemotherapy to eliminate the remaining cancer cells that survive RF ablation.

For thermoablated tumors, the desired site of action for drugs is located at the boundary of the thermoablated and nonablated tissue, where residual viable

Correspondence to: J. Gao; e-mail: jmg23@po.cwru.edu
Contract grant sponsor: the Whitaker Foundation; contract grant number: RG-99-0342

cancer cells are most likely present. For intratumoral drug delivery to be effective, it is necessary that drug molecules be able to penetrate through the ablated tissue from the polymer millirod and reach therapeutic concentrations at the ablation boundary. Questions regarding the penetration distance and the time to achieve drug therapeutic concentrations at the site of action need to be addressed. In this study, we report the transport properties of an anticancer drug, doxorubicin, in thermoablated rabbit livers *in vivo*. Doxorubicin is an anthracyclin-based antitumor agent that displays a broad activity against liver cancers.[6,7] Results demonstrate that doxorubicin was able to reach the therapeutic level at the ablation boundary after 24 h. In addition, comparison of the distribution dynamics of doxorubicin in ablated and normal tissues provides significant insights in understanding the drug transport processes *in vivo*.

MATERIALS AND METHODS

Materials

Poly(D,L-lactide-*co*-glycolide) (PLGA, lactide: glycolide = 1:1, MW = 50,000 Da, inherent viscosity 0.65 dL/g) was purchased from Birmingham Polymers, Inc. (Birmingham, AL). Doxorubicin was purchased from Bedford Labs (Bedford, OH). Polyethylene glycol (PEG, MW = 5, 000 Da) was purchased from Aldrich Chemical Company, Inc. (Milwaukee, WI). Phosphate-buffered saline (PBS) and methylene chloride were obtained from Fisher Scientific (Pittsburgh, PA).

Fabrication and characterization of polymer millirods *in vitro*

Polymer millirods containing 10% doxorubicin, 50% PEG, and 40% PLGA were fabricated by a compression-heat molding procedure described previously.[8] Briefly, doxorubicin solution (2 mg/mL, also containing 0.9% NaCl) was first dialyzed in distilled water to remove the NaCl. The desalted solution was lyophilized to obtain the purified solid particles of doxorubicin. The drug particles were mixed with PLGA microspheres (average diameter 5 μm) and PEG powder. The mixed particles were vortexed and placed in a Teflon tube and molded into a polymer millirod at a compression pressure of 4.6×10^6 Pa and a fabrication temperature at 70°C for 5 min. The *in vitro* release study was carried out in PBS buffer (pH 7.4) at 37°C by an UV-Vis spectrophotometer (Lambda 20 model, Perkin-Elmer Corp.). The Beer–Lambert law was used to calculate the agent concentration at its maximum absorption wavelength (λ_{max} = 480.8 nm) at each time point. The cumulative mass of the released agent was calculated by summing the individual mass after each sample removal.

Correlation of doxorubicin fluorescence intensity with its tissue concentration

A calibration curve correlating fluorescence intensity with doxorubicin concentration in liver tissue was first established. In this set of experiments, a piece of healthy rabbit liver was frozen and sliced by a cryostat microtome (Microm 505E model) at 100-μm thickness. The size of the liver slice was controlled approximately at 15×30 mm^2, and the weight of each slice was measured and recorded immediately after cutting. A series of doxorubicin solutions were prepared at concentrations of 1, 5, 10, 25, 50, 100, 200, and 500 μg/mL. Doxorubicin-containing liver slices were prepared by spreading 40 μL of doxorubicin solution on the surface of the liver slice on a glass slide. Three samples were prepared for each concentration. The liver slices were placed in a black box to allow water evaporation. The weight of the liver slice was monitored until it returned to the original weight, and then the slice was sealed by the mounting media and covered with a cover slip. Three doxorubicin-free liver slices were also prepared as control samples for the liver background. All the slices were placed on a fluorescence imager (FluorImager™ SI model, Molecular Dynamics, Inc.) and scanned simultaneously. The fluorescence images were saved in TIFF format and ImageJ software (freeware available from NIH) was used to calculate the average fluorescence intensity of each liver slice. Net fluorescence intensity (NFI) was calculated by subtracting the fluorescence intensity of drug-free liver slices from drug-containing slices. The value of NFI was plotted as a function of doxorubicin concentration in the liver tissue. The least-squares curve fit leads to a correlation equation: $NFI = 586*[Doxorubicin]^{0.51}$, which was used in later experiments to convert fluorescence intensity to doxorubicin tissue concentration. To estimate the sensitivity limit for doxorubicin detection, we determined the experimental noise (a combination of electronic noise due to imager and sample noise due to sample variation) for each concentration. We found that the experimental noise is comparable to the fluorescence signals as produced by 0.6 μg/g of doxorubicin concentration.

RF ablation of rabbit livers and implantation of polymer millirods

The animal procedure follows the NIH Guidelines and an animal protocol approved by the Institutional Animal Care and Use Committee (IUCAC) at Case Western Reserve University. Male New Zealand white rabbits (3–3.5 kg) were anesthetized with a cocktail of ketamine, xylazine, acepromazine, and atropine. The abdomen was shaved and swabbed with a solution of betadine prior to the start of surgery. The liver was exposed through an incision in the midsection. The medial lobe of the liver was ablated with a 19-gauge needle electrode (Radionics®, Burlington, MA) at 90 ± 3°C for 3 min to create an ablation zone of approximately 6 mm in diameter. This RF ablation procedure is similar to those described previously.[9,10] A short segment of a doxorubicin millirod was implanted into the ablated lobe. An identical rod segment was implanted into the right lobe, which was first

punctured with an 18-gauge hypodermic needle. A small piece of fat was sutured on top of both implantation sites to prevent the implants from slipping out. Following the surgery, the animals were monitored periodically to assure their health and safety.

Analysis of drug distribution profiles

At different time points, the rabbits were sacrificed and the livers were removed for drug distribution and histology analysis. First, the millirod was removed from the implantation site to determine the remaining amount of doxorubicin inside the millirod. To mark the implantation site and orientation, a blue liquid latex solution was injected into the cavity, followed by a small length of plastic tubing, which extended past the surface of the liver. The livers were frozen in a −80°C freezer. During sample preparation, the tubing was removed and livers were trimmed with a long blade to the starting end of the millirod. The liver sample was then mounted on a cryostat chuck with O.C.T. embedding medium (Miles Inc., Elkhart, IN) and cut into slices for drug distribution and histology studies. All slices were cut perpendicular to the long axis of the millirod. Alternating slices for drug distribution and histology studies were prepared, which permits later image registration between drug distribution profiles and histology images. Slices for drug distribution study were cut into 100 μm-thick slices while the ones for histology were cut into 2-mm slices. The thicker slices are necessary to obtain large tissue sections (~2 cm in diameter) by the histology facility on campus. The liver slices for drug distribution analysis were scanned by the fluorescence imager, and the fluorescence intensity in the image was converted to drug concentration based on a predetermined calibration curve (see above). The liver slices were also examined at higher magnifications by a fluorescence microscope (Nikon Eclipse TE300 model).

Histology analysis

The histology slices were first placed in 10% formalin solution for fixation. After fixation, the samples were embedded in paraffin, sliced to a thickness of 5 μm, and stained with hematoxylin and eosin (H&E). The H&E sections were alternated with unstained sections preserved for TUNEL staining. For the TUNEL assay, standard procedures from the manufacturer's guidelines (Oncogene TdT-FragEL™ kit) were followed. Briefly, the unstained sections were deparaffinized with two 10-min xylene washes and hydrated with sequential ethanol dilutions. The slices were incubated with proteinase K in Tris buffer (pH 8) and then incubated at 37°C with the TUNEL reaction mixture and diaminobenzidine stain. The sections were counterstained with hematoxylin, dehydrated in ethanol, fixed on slides, and covered with cover slips for analysis. The assay allowed the recognition of apoptotic nuclei by binding terminal deoxynucleotidyl transferase (TdT) to exposed 3′-OH ends of DNA fragments generated as a response to the apoptotic cascade. The binding catalyzed the addition of biotin-labeled and unlabeled deoxynucleotides. Biotinylated nucleotides were then detected with a streptavidin–horseradish peroxidase conjugate and tagged with diaminobenzidine. The apoptotic nuclei appeared brown on the sections in contrast with the counterstain, hematoxylin, which appeared blue.

RESULTS AND DISCUSSION

Dynamics of doxorubicin distribution in rabbit livers *in vivo*

In this study, we used polymer millirods with burst release kinetics to examine the drug transport properties in thermoablated and nonablated liver tissues. *In vitro* release studies in PBS buffer at 37°C showed that the time ($t_{1/2}$) for 50% release of loaded doxorubicin was 0.5 h and more than 90% of doxorubicin was released after 1.5 h. Polymer millirods were implanted in either nonablated or ablated livers and, at different implantation times, the liver was harvested and the drug distribution profiles were obtained perpendicular to the long axis of the millirod. Figure 1 illustrates the two-dimensional doxorubicin distribution profiles in nonablated and thermoablated liver tissues at different implantation times. Figure 1(A–E) utilizes pseudocolor images constructed in MatLab 5.3 to provide a better illustration of concentration distribution. The red color in the images corresponds to a higher doxorubicin concentration. White dashed lines in Figure 1(C–E) represent the ablated–normal tissue boundary, which was obtained by comparing the fluorescence image with an optical image of histology slides where this boundary is well defined (see histology section below).

Figure 1(A,B) shows that in normal livers, doxorubicin distribution is limited to the implantation site, and almost no doxorubicin is detected 2 mm away from the millirod–tissue interface. This observation is similar to those from Dr. Saltzman's lab on tissue distribution of carmustine (BCNU, another anticancer drug) in brain tissue.[11,12] We analyzed the doxorubicin content in the retrieved polymer millirods and results showed that only 1.2 and 0.6% of doxorubicin remained in the millirods 24 and 48 h after implantation, respectively. These results indicate that high blood perfusion leads to the depletion and narrow distribution of doxorubicin in nonablated liver tissue.

The patterns of doxorubicin distribution in ablated tissue [Fig. 1(C–E)] are drastically different from those in nonablated tissue [Fig. 1(A,B)]. At all three time points (4, 24, 48 h), drug penetration in ablated tissue is significantly larger than that in nonablated tissue. We believe that this larger area of distribution is primarily due to the destruction of liver vasculature by

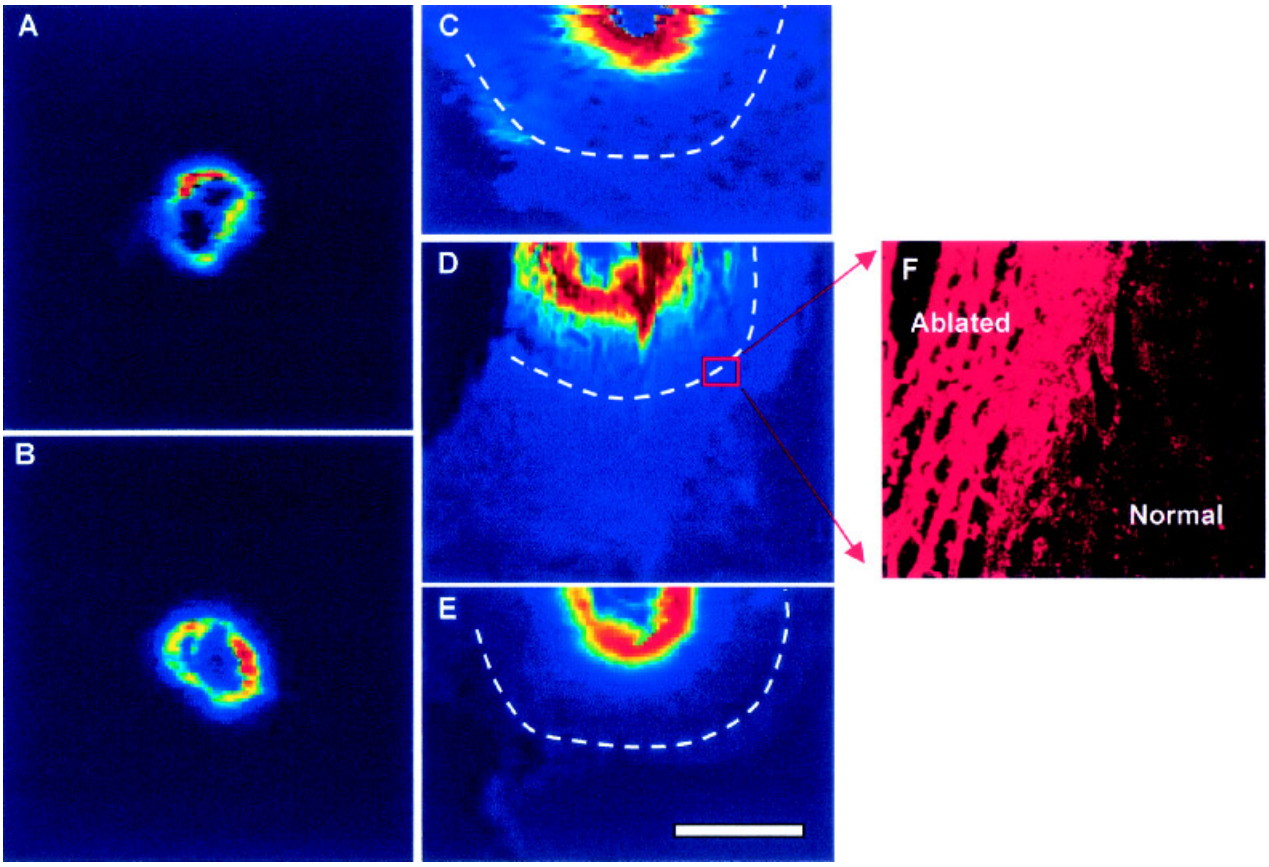

Figure 1. Fluorescence imaging of doxorubicin distribution in normal and ablated rabbit livers. (A, B) Doxorubicin distribution in normal livers 24 and 48 h after millirod implantation, respectively. (C, D, E) Doxorubicin distribution in ablated livers 4, 24, and 48 h after millirod implantation, respectively. The white dashed lines in (C–E) represent the ablated–normal tissue boundary. Due to the large distribution pattern in ablated livers, only half of the liver slice is shown in (C–E). The scale bar (3 mm) in (E) applies to (A–D) as well. (F) Fluorescence microscopy image (4×) of doxorubicin at the normal–ablated tissue boundary 24 h after millirod implantation. See text for detailed description. [Color figure can be viewed in the online issue, which is available at www.interscience.wiley.com.]

thermoablation (as evident from histology analysis below), which hampers the drug washout by liver perfusion. Under such circumstances, drug diffusion becomes the dominant transport process in the ablated tissue. Detailed examination shows that the distribution pattern in the ablated tissue changed with time following millirod implantation. The distribution pattern at 24 h [Fig. 1(D)] is larger than those at 4 [Fig. 1(C)] and 48 h [Fig. 1(E)]. Analysis of the retrieved millirods showed that 5.1 and 0.9% of doxorubicin remained in the millirods after 24 and 48 h, respectively. The depletion of doxorubicin inside the millirods after 24 h (only 5.1% remaining) can help to explain the decrease in distribution pattern at 48 h [Fig. 1(E)].

In addition to the macroscopic fluorescence imaging study, we also used fluorescence microscopy to examine the liver slices. Figure 1(F) shows the true fluorescence image at the boundary of ablated and nonablated tissue. Because the two peak emission wavelengths of doxorubicin are 560 and 593 nm, the fluorescence image shows the red color. The more obvious color contrast between the ablated and nonablated regions in Figure 1(F) compared with 1(D) is due to the different color scales, which reflect a concentration range of 0–50 μg/g in 1(F) (true color) and 0–500 μg/g in 1(D) (assigned color). In Figure 1(F), the ablated region is represented by loose cellular structures that resemble the histology sections (Fig. 3).

Quantitative pharmacokinetic analysis of doxorubicin distribution

Figure 2(A) provides a series of quantitative profiles correlating doxorubicin concentration ([DXR]) with distance from the millirod–tissue interface. Each profile was obtained by averaging four different radial profiles in a 2D image. Results in Figure 2(A) show that the doxorubicin concentrations at the millirod/tissue interface were smaller in nonablated liver tissue than those in ablated tissue. The area of distribution was much wider in ablated tissue than in nonablated

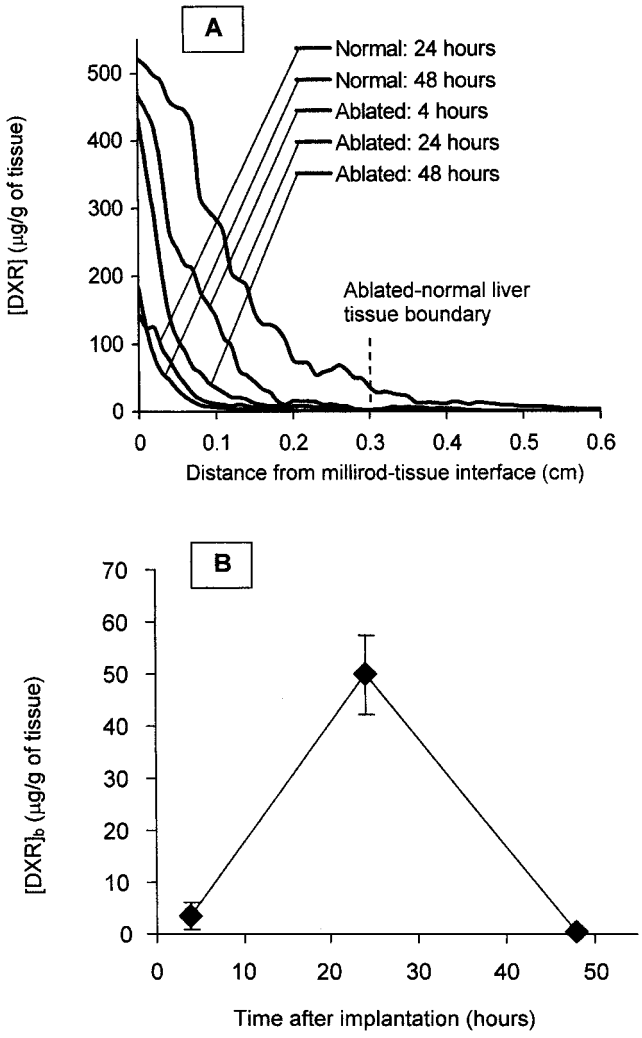

Figure 2. Pharmacokinetic analysis of doxorubicin distribution in liver tissues. (A) Quantitative doxorubicin concentration ([DXR]) vs. distance relationships at different experimental conditions. (B) Doxorubicin concentration at the ablated–normal tissue boundary ($[DXR]_b$) at 4, 24, and 48 h after millirod implantation.

tissue, demonstrating a higher percentage of drug retaining in the ablated tissue. Ridge and coworkers have reported that the cytotoxic concentration of doxorubicin to the rabbit liver VX-2 tumors (this is also our animal tumor model) is 6.4 μg/g.[13] Based on the quantitative [DXR]–d curves, we determined the values of therapeutic distance (TD, the distance at which [DXR] is equal to 6.4 μg/g) were 1.2 ± 0.5 and 1.0 ± 0.1 mm in nonablated livers at 24 and 48 h, respectively. Similarly, the values of TD were 3.1 ± 0.4, 5.2 ± 0.8, and 2.5 ± 0.3 mm in ablated livers at 4, 24, and 48 h, respectively.

Based on Figure 2(A), we obtained the correlation of doxorubicin concentration ($[DXR]_b$) at the ablated–normal tissue boundary as a function of the implantation time [Fig. 2(B)]. As we previously described, the ablated–normal tissue boundary is the desired site of action because most cancer cells will survive in this region. The $[DXR]_b$–t curve describes the relationships between the drug concentrations vs. time at the site of action. This analysis is similar to the concept of plasma drug concentration–time curve widely used in clinical pharmacokinetic studies for systemic chemotherapy.[14] Results from Figure 2(B) show that the value of $[DXR]_b$ reached 3.3 ± 2.6 μg/g at 4 h. At 24 h, the value of $[DXR]_b$ reached a maximum of 49.8 ± 7.5 μg/g concentration, which is significantly higher than the cytotoxic concentration of doxorubicin (6.4 μg/g) to liver VX-2 cells. The value of $[DXR]_b$, however, dropped to 0.4 ± 0.1 μg/g after 48 h as a result of the depletion of doxorubicin in the polymer millirod. To maintain the value of $[DXR]_b$ at the therapeutic level, polymer millirods with sustained release kinetics will be necessary.

Histology analysis

Figure 3(A) shows the H&E staining of the ablated liver tissue 48 h following the implantation of a doxorubicin millirod. Upon gross examination, three distinctive regions were identified:

1. The necrotic core (arrowheads), which is a result of thermoablation. This region was identified by the darker pink color, lack of a defined nuclear structure, and destroyed sinusoidal vasculature. The destroyed vasculature eliminates blood perfusion in the ablated regions. Consequently, drug transport in this region is mostly diffusion based.
2. The inflammatory region (arrow), which is easily recognized by the presence of dark nuclei of the inflammatory cells (e.g., leukocytes). These cells accumulated in the area of injury as part of wound-healing response.[15]
3. The viable hepatocyte region, which is located at the bottom right corner of the section. These cells have well-defined cytoplasm and nucleus, and the sinusoidal vasculature is maintained.

The TUNEL section of the same area [Fig. 3(B)] also shows the three distinctive regions in the ablated tissue. The necrotic region appears light brown, and the inflammatory and normal tissue regions appear blue due to the hematoxylin counterstain to viable inflammatory cells and hepatocytes. Zones 1, 2, and 3 marked on the TUNEL overview section [Fig. 3(B)] are areas of interest at the interface of the ablated and viable tissue area. The necrotic cells are shown closer in Figure 3(B-1). Their nuclei and cytoplasms are slightly stained brown. The brown staining of necrotic cells is a result of the nonspecific binding of the TdT–DAB complex to the DNA released into the necrotic cell cytoplasm. This is a common problem encountered with the TUNEL assay; however, it can

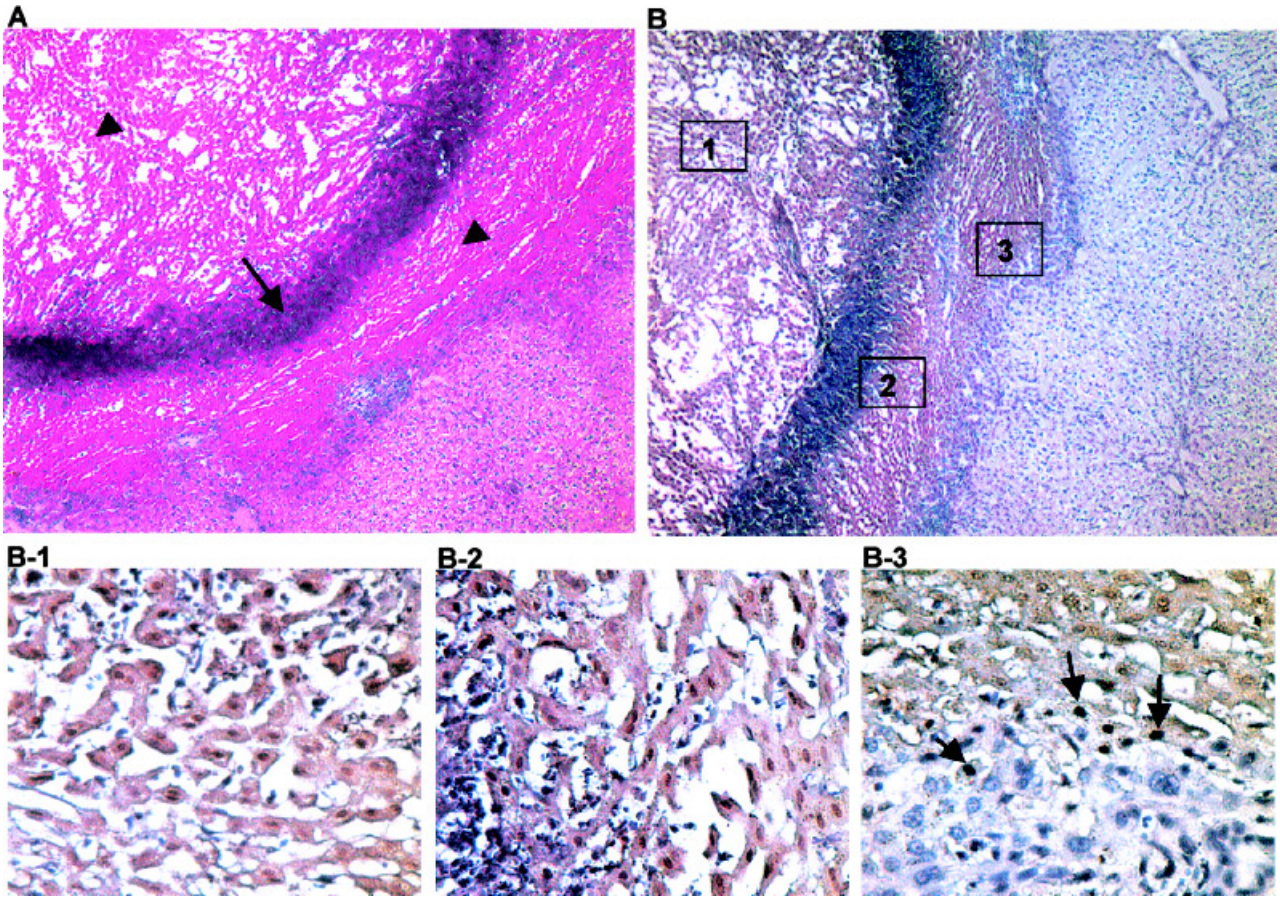

Figure 3. Histological evaluation of ablated rabbit livers after local delivery of doxorubicin for 48 h. The implantation site is located beyond the upper left corner of the image. (A) H&E staining (4×) shows three distinctive regions at the ablated implantation site: necrotic core (arrowheads), inflammatory region (arrow), and normal liver tissue at the bottom right corner. (B) Overview of TUNEL section (4×) showing the same three regions as 3(A). The necrotic hepatocytes appear brown due to the nonspecific TdT–DAB binding to DNA in cytoplasm. Three areas of interest are shown at higher magnification (40×): (B-1) Necrotic core with lightly brown nuclei and cytoplasm. (B-2) Interface between the inflammatory infiltrate (left) and necrotic hepatocytes. (B-3) Distal border of ablated area interfacing with viable tissue shows apoptotic cells (arrows) implying a heat-induced cell death. [Color figure can be viewed in the online issue, which is available at www.interscience.wiley.com.]

be used to the advantage of this study in identifying the cell necrosis induced by thermoablation instead of solely relying on morphometric analysis of the H&E sections. The interface between the infiltrating leukocytes and necrotic cells is shown in Figure 3(B-2). The migration of the leukocytes still belongs to the acute inflammation stage of the wound-healing process. Figure 3(B-3) shows the distal interface of the ablation injury and viable hepatocytes. The cells marked with arrows appear to be apoptotic, with their nuclei staining a dark brown color and cytoplasms reflecting little nonspecific staining.

These results demonstrate that the interface of the ablated and viable liver tissue can be easily identified with both H&E and TUNEL staining. The TUNEL results further demonstrate that apoptosis did occur at the distal ablation boundary, where the doxorubicin molecules reached therapeutic levels [24-h time point in Fig. 2(B)]. However, it is possible that the apoptosis may not be the result of doxorubicin-induced toxicity, and may instead be attributed to a heat-induced mechanism. At the ablation boundary, the temperature may have been elevated sufficiently to induce apoptosis but not high enough to cause coagulative necrosis.[16] To distinguish these two possible mechanisms, we examined the tissue sections of *nonablated* livers where the same doxorubicin millirod was implanted for 48 h. The TUNEL assay revealed no apoptotic cells surrounding the implant (data not shown), which indicates that the drug-induced toxicity to normal hepatocytes is very slight in our system. This result is reasonable because doxorubicin is a cell cycle-specific agent that attacks cells at the S-phase, but the low proliferation ratio in normal hepatocyte population (1 in 15,000 cells)[17] decreases the chances of an apoptotic event. We expect that the apoptotic event will be much more frequent in tumor tissues where cancer cells proliferate at a much higher rate. Current

work is in progress to evaluate the intratumoral delivery of doxorubicin in a RF ablated rabbit VX-2 liver tumors.

CONCLUSIONS

Results from this study have many important implications to establish intratumoral drug delivery for local cancer chemotherapy. First, not only can RF ablation provide an instant kill to the major population of the cancer cells, it can also destroy the tumor vasculature to minimize drug loss due to perfusion while maximizing drug penetration to achieve sufficient therapeutic margin. This is supported by the increase in the therapeutic distance from 1.2 mm in nonablated livers to 5.2 mm in ablated livers. This observation is important because without RF ablation, intratumoral drug delivery may be limited as a single treatment due to insufficient drug penetration. Second, this study demonstrates that the anticancer drug, doxorubicin, can successfully penetrate through the ablated tissue and reach the therapeutic concentration within a reasonable time frame [<24 h, Fig. 2(B)]. This is critical for the combination therapy (RF ablation + intratumoral drug delivery) to be effective. Third, to achieve maximal drug efficacy at the ablation boundary, polymer millirods with dual release kinetics—an initial burst release followed by sustained release of drugs—are probably desirable. In such a design, the initial burst provides a sufficiently high dosage of the drug to quickly reach the therapeutic concentration at the ablation boundary, and the sustained release will maintain the therapeutic concentration for a prolonged period of time. This design will be necessary especially in the use of cell cycle-specific drugs (e.g., doxorubicin) to kill slow proliferating cancer cells that may have long cell cycles. Fourth, mass transport models can be used to describe the dynamics of drug distribution in ablated and surrounding tissues. These models can potentially provide a rational basis to permit an optimal design of the burst dose and sustained release rate to achieve a safe and effective local cancer chemotherapy.

References

1. Lewin JS, Connell CF, Duerk JL, Chung YC, Clampitt ME, Spisak J, Gazelle GS, Haaga JR. Interactive MRI-guided radiofrequency interstitial thermal ablation of abdominal tumors: Clinical trial for evaluation of safety and feasibility. J Magn Reson Imaging 1998;8:40–47.
2. Djavan B, Susani M, Shariat S, Zlotta AR, Silverman DE, Schulman CC, Marberger M. Transperineal radiofrequency interstitial tumor ablation (RITA) of the prostate. Technol Urol 1998;4:103–109.
3. Goldberg SN, Gazelle GS, Compton CC, Mueller PR, McLoud TC. Radio-frequency tissue ablation of VX2 tumor nodules in the rabbit lung. Acad Radiol 1996;3:929–935.
4. Bartolozzi C, Crocetti L, Cioni D, Donati FM, Lencioni R. Assessment of therapeutic effect of liver tumor ablation procedures. Hepatogastroenterology 2001;48:352–358.
5. Dodd GD III, Soulen MC, Kane RA, Livraghi T, Lees WR, Yamashita Y, Gillams AR, Karahan OI, Rhim H. Minimally invasive treatment of malignant hepatic tumors: At the threshold of a major breakthrough. Radiographics 2000;20:9–27.
6. Ramirez LH, Munck JN, Bognel C, Zhao Z, Ardouin P, Poupon MF, Gouyette A, Rougier P. Pharmacology and antitumour effects of intraportal pirarubicin on experimental liver metastases. Br J Cancer 1993;68:277–281.
7. Rougier P, Munck JN, Elias D, Herait P, Bognel C, Gosse C, Lasser P. Intra-arterial hepatic chemotherapy with pirarubicin. Preclinical and clinical studies. Am J Clin Oncol 1990;13(Suppl 1):S1–S4.
8. Feng Q, Szymanski A, Gao J. Fabrication and characterization of controlled release poly(D,L-lactide-co-glycolide) millirods. J Biomed Mater Res 2001;55:512–522.
9. Merkle EM, Boll DT, Boaz T, Duerk JL, Chung YC, Jacobs GH, Varnes ME, Lewin JS. MRI-guided radiofrequency thermal ablation of implanted VX2 liver tumors in a rabbit model: Demonstration of feasibility at 0.2 T. Magn Reson Med 1999; 42:141–149.
10. Boaz TL, Lewin JS, Chung YC, Duerk JL, Clampitt ME, Haaga JR. MR monitoring of MR-guided radiofrequency thermal ablation of normal liver in an animal model. J Magn Reson Imaging 1998;8:64–69.
11. Fung LK, Shin M, Tyler B, Brem H, Saltzman WM. Chemotherapeutic drugs released from polymers: Distribution of 1,3-bis(2-chloroethyl)-1-nitrosourea in the rat brain. Pharm Res 1996;13:671–682.
12. Strasser JF, Fung LK, Eller S, Grossman SA, Saltzman WM. Distribution of 1,3-bis(2-chloroethyl)-1-nitrosourea and tracers in the rabbit brain after interstitial delivery by biodegradable polymer implants. J Pharmacol Exp Ther 1995;275:1647–1655.
13. Ridge JA, Collin C, Bading JR, Hancock C, Conti PS, Daly JM, Raaf JH. Increased adriamycin levels in hepatic implants of rabbit VX-2 carcinoma from regional infusion. Cancer Res 1988;48:4584–4587.
14. Benet LZ, Kroetz DL, Sheiner LB. Pharmacokinetics. In: Hardman JGLL, Molinoff PB, Ruddon RW, editors. Goodman & Gilman's The pharmacological basis of therapeutics, 9th ed. New York: McGraw-Hill Health Professions Division; 1996. p 3–27.
15. Anderson J. Mechanisms of inflammation and infection with implanted devices. Cardiovasc Pathol 1993;2(Suppl):33s–41s.
16. Jeschke MG, Low JF, Spies M, Vita R, Hawkins HK, Herndon DN, Barrow RE. Cell proliferation, apoptosis, NF-kappaB expression, enzyme, protein, and weight changes in livers of burned rats. Am J Physiol Gastrointest Liver Physiol 2001;280: G1314–G1320.
17. Martinez–Hernandez A. Repair, regeneration and fibrosis pathology, 2nd ed. Philadelphia: J.B. Lippincott; 1994. p 69–95.